SINET: Ethiop. J. Sci., 45(2): 132–142, 2022 ISSN: 0379–2897 (PRINT)
 eISSN: 2520–7997

Date received: January 31, 2022; Date revised: August 03, 2022; Date accepted: August 05, 2022
DOI: *https://dx.doi.org/10.4314/sinet.v45i2.2*

The effect of surface plasmonic resonances on magneto-plasmonic Fe_3O_4@Ag spherical core-shell nanocomposites

Kinde Yeneayehu*, Teshome Senbeta and Belayneh Mesfin

Department of Physics, Addis Ababa University, Addis Ababa, Ethiopia. E-mail: kinde.yeneayehu@aau.edu.et

ABSTRACT: In this study, the effect of plasmon resonance on magneto-plasmonic Fe_3O_4@Ag spherical core-shell nanocomposite enclosed in a dielectric host medium is theoretically investigated by applying electrostatic approximation (ESA) and Maxwell-Garnet effective medium theories to obtain magneto-optical parameters such as; effective electric permittivity and magnetic permeability as well as the corresponding extinction cross-sections. Likewise, for a fixed size of QDs (of radius $a_s = 10$ nm) numerical analysis was performed to determine the plasmonic resonance effect by varying the parameters such as the metal fraction (β) and the dielectrics (ε_h) of the host medium on the magneto-plasmonic nanostructures (NSs). The results depict that graphs of absorption, scattering, and extinction cross-sections as a function of wavelength have two positions of resonance peaks. The first set of peaks are in the ultraviolet (UV) and the second located in visible regions. These peaks originated from the strong coupling between a regular periodic vibrations of surface plasmons of silver (Ag) with the excitonic state of the dielectric/semiconductor at the internal (Fe_3O_4@Ag) and external (*Ag*/host) interfaces. As β increases, the absorption and scattering cross-sections are blue-shifted in the first peak and red shifted the second set of peaks. Similarly, as ε_h increases or as β decreases, the sets of resonance peaks for extinction cross-section gets enhanced; while keeping one of these parametric quantities fixed at once. The resulting surface plasmon resonance effect might be utilized in a variety of applications that combines both the plasmonic and magnetic core-shell nanostructures ranging from UV to Visible spectral regions.

Keywords/phrases: Core-shell, Dielectric Function, Extinction Cross-section, Surface Plasmon Resonance

INTRODUCTION

A great attention has been given to the development of nanomaterials as they exhibit unique material properties as compared to their bulk counterpart. These unique properties include optical, magnetic, specific heat, melting point, surface activities, chemical and biological properties (Chingsungnoen and Dasri, 2017). Nanomaterials form heterogeneous structures composed of a noble metal and a semiconductor. These peculiar type of systems offer to design materials with novel and unique physical and chemical properties. As isolated systems, the optical properties of semiconductor quantum dots (QDs) and noble metal nanoparticles (NPs) are characterized by excitons and plasmons, respectively. In both cases, the required wavelengths to produce such excitations are governed mainly by the nanoparticle nature, size, shape, and local environment (Ezequiel, *et al.*, 2013).

As an important class of nanomaterials, core-shell nanoparticles (NPs) that integrate two dissimilar materials with distinct functionalities have attracted more and more attention, since they have emerged at the frontier between materials chemistry and many other fields, such as biomedical, optics, catalysis. Because core-shell NPs enable the synergistic coupling of the two constituents, they could offer the modified properties by changing either the constituting materials or the core to shell ratio. Therefore, this nanostructure can meet the diverse application requirements. Among various core-shell NPs, magnetic/noble metal hybrid NPs have been widely studied as they possess intriguing magnetic/plasmonic and magnetic/catalytic properties, and they can be used in many fields, for example optical devices, chemical reactions as magnetically recyclable catalysts, bioimaging, targeted drug delivery. *Ag*-based magnetic hybrid NPs play an important role in specialty chemistry, physics and material science. By varying the size of the Fe_3O_4 cores and Ag shell,

*Author to whom correspondence should be addressed.

the optical properties of nano-hybrids can be tuned in a broad spectral ranges (Fan,*et al.* 2019).

Magnetic and/or plasmonic nanostructures demonstrate multiple properties not present in individual nanomaterials. Such materials offer the advantage of being manipulated by an external magnetic field, showing tunable optical properties being adjustable in accordance with modifying shell thickness. Experimental and computational studies by (Kheradmand, *et al.,* 2020) shows that the higher the magnetization in magnetic core nanoparticles, the more is the suitable response toward the exposed magnetic field and the higher the effectiveness in nano-medical diagnostics. Magnetic-plasmonic core shell NPs possess dual magnetic and plasmonic properties and have widespread applications in biomedical fields. The magnetic cores such as iron-oxide (IO) are greatly desired for applications such as magnetic separation, magnetic resonance imaging or magnetic guided drug delivery. The IO-cores can be chemically stabilized by coating them with noble metals, which not only provides a chemically inert surface, but also introduces interesting plasmonic properties which can be utilized for sensing, imaging, and photothermal therapy (Shweta *et al.,* 2019).

The possibility of building new nanostructures by mixing noble metals *Ag* and magnetic Fe_3O_4 nanoparticles (NPs) opens up a wide spectrum of desirable synergistic and complementary effects. One of the challenges is the conjunction of these two dissimilar materials in a controlled way. Thus, great efforts have been made on synthetic routes to command the bonding of the heteroparticle (Ahmad, *et al.,* 2015). The plasmon resonance wavelength, light scattering, absorption and extinction cross-section of core-shell are affected by shell thickness, core diameter, electronic properties of shell and surrounding environment at outer interface between the surface and incident light, and inner interface between metal and semiconductor. Localized surface plasmon resonance gives rise to an enhancement of electric field, localization of energy at nanometer scale, and strongly enhanced absorption and scattering of light.

Magnetic nanoparticles with a core-shell structure promises for many applications due to their multi-functionality including optical, electronic, and magnetic properties (Poedji Loekitowati Hariani, *et al.,* 2013). In particular, these $Fe_3O_4@Ag$ core-shell NPs combine the magnetic and optical properties of Fe_3O_4 and Ag together, exhibiting great potential in the fields of bio-related separation, ultrasensitive detection and cellular imaging (Fan, 2019). Fe_3O_4 (Magnetite) is one of the magnetic nanoparticles. Different reports are demonstrating that magnetic Fe_3O_4 can be used for waste water purification, such as to adsorb arsenite, arsenate, cadmium, nickel (Luciano, *et al.,* 2013; Ana, *et al.,* 2019) used to remove alkalinity and hardness, desalination, decolourization of pulp mill effluent and removal of natural organic compounds. After adsorption, Fe_3O_4 can be separated from the medium by a simple magnetic process (Poedji, *et al.,* 2013).

Noble metals nanoparticles, such as Ag and Au, strongly absorb light in the visible region due to coherent oscillations of the metal conduction band electrons in strong resonance with visible frequencies of light. This phenomenon is known as surface Plasmon resonance (SPR) and is highly dependent on NPs size, shape, surface, and dielectric properties of the surrounding medium. Light absorbed by nanoparticles is readily dissipated as heat. Due to their large absorption cross sections, plasmonic NPs can generate a significant amount of heat and increase temperatures in their vicinities (Ana, *et al.,* 2019; Kerker, 1969; Papavassiliou, 1979; Huffman, 1998; Vollmer, 1995).

Silver NPs have been applied as a broad spectrum and highly effective bactericide. The antibacterial mechanism is associated to the release of silver ions. For medical applications, an $Ag@Fe_3O_4$ core-shell structure allows one to add a magnetic functionality to silver properties. Such nanostructure could lead to interesting advances to solve the lack of bio-compatibility of silver, eliminating its contact with tissues (iron-oxide can be considered biocompatible, at least up to the mg/ml range). However, an intriguing behavior was observed on $Ag@Fe_3O_4$ NPs: its bactericidal efficiency is stronger than $Ag-Fe_2O_3$ hetero-dimers or plain Ag (Maria, *et al.,* 2014; Morones, *et al.,* 2005; Xu, *et al.,* 2009).

Surface plasmon absorption has been observed for silver particles in various media, including aqueous solutions, gelatin and glass. Size effects exhibited by nearly spherical silver particles are similar to those for gold. While, extinction is the attenuation of an electromagnetic wave by scattering and absorption as it traverses a particulate medium. In homogeneous media the dominant attenuation mechanism is usually absorption. Comparison of extinction spectra for small particles of various sizes with absorption

spectra for the bulk parent material reveals both similarities and differences (Bohren, 1998).

To investigate the optical properties and response (absorption and scattering) of NPs with light (electromagnetic radiation) interaction, one has to measure the effective dielectrics, ε_{eff}, and permeability, μ_{eff}, (Challa, 2013). In this paper, we studied the effect of plasmon resonance on the theoretically modelled spherical Fe_3O_4@Ag core-shell NPs. Silver nanoparticle was selected as a shell on magnetite nanospheres, due to its nontoxic, strong absorption in the UV and visible spectrum (Vladimir, *et al.*, 2013) and surface plasmon resonance (SPR) which plays a great role in determining the optical response of nanoparticles.

The paper is structured as follow: In Section 2, the effective dielectrics and permeability of the theoretically modelled magnetic-semiconductor/metal core-shell spherical NPs embedded in a dielectric host matrix are derived. In Section 3, equations for the effective polarizabilities, absorption cross-section and scattering cross-section are derived. The numerical results are presented and discussed in Section 4. Detailed analysis of the effect of plasmonic resonance on Fe_3O_4@Ag core-shell NPs, namely the absorption cross-section, scattering cross-section and extinction cross-section are presented. Finally, concluding remarks are presented in Section 5.

Theoretical model

Interaction of electromagnetic radiation with particles is well studied. Theoretical studies on the optical properties of multilayer spherical nanoparticles are reported in lots of literatures. In particular, for our general discussion, in this section we expose the basic concepts of the theory for scattering of electromagnetic waves by core-shell materials following the considerations of a model of Fe_3O_4@Ag spherical core-shell NPs, which is composed of magnetic-half metallic iron (III) oxide (Fe_3O_4) core of radius a_c and an outer metallic (Ag) shell of radius a_s embedded in a dielectric host matrix as shown in Fig. 1, where $a_c < a_s$. Because of the core material is magnetic with permeability, $\mu \gg 1$, the magneto-optical properties of the system requires determination of its effective dielectrics ε_{eff} and permeability μ_{eff}. Based on electrostatic approximation and the Maxwell-Garnet effective medium theory, theoretical analysis have been done to derive ε_{eff} and μ_{eff}. Moreover, using these theoretically determined values, calculations has been done on the magneto-optical parameters such, as the electric polarizability, absorption, and scattering cross-sections.

Effective Dielectric Function and Magnetic Permeability

The effective dielectric function of the core-shell composite material given by (Kinde, *et al.*, 2021; Gashaw, *et al.*, 2019; Leta, *et al.*, 2015):

$$\varepsilon_I = \varepsilon_s \frac{\varepsilon_c\left(\frac{3}{\beta}-2\right)+2\varepsilon_s}{\varepsilon_c+\varepsilon_s\left(\frac{3}{\beta}-1\right)}, \qquad (1)$$

where $\beta = 1 - \nu_f$ is the volume fraction of the metal coated spherical core-shell nanoparticle, and $\nu_f = \left(\frac{a_c}{a_s}\right)^3$.

Here, we consider a system composed of a finite number of core-shell NPs uniformly dispersed in a host matrix, as shown in Fig. 1.

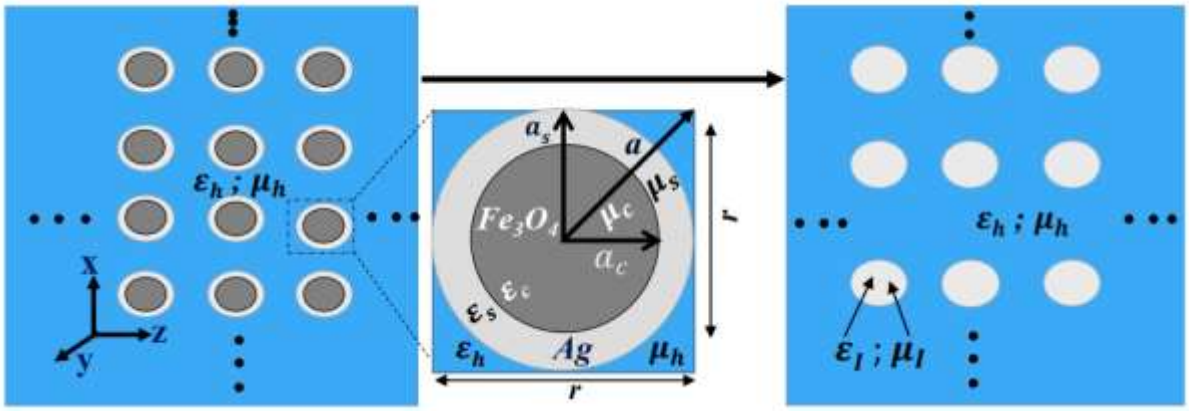

Figure 1. Schematic of a core-shell spherical NPs embedded in a matrix. The dielectrics and permeabilities are ε_c, μ_c for the core, ε_s, μ_s for the shell, and, ε_h, μ_h for the host matrix, respectively. Also, a_c, a_s are the radii of the core and the shell, $r = 2a_s$ is the diameter of core-shell, and a is the distance from the center of the NP to an observation point.

Suppose N is the density number of the inclusions (NPs) in the system, then the effective polarizability and permittivity of the system can be described by using the Clausius-Mossotti relation together with the Maxwell-Garnet mixing formula. Accordingly, the electric polarizability and the effective dielectrics are related by (Starodubtcev, *et al.*, 2013),

$$\frac{N\alpha}{3} = \frac{\varepsilon_{eff} - \varepsilon_h}{\varepsilon_{eff} + 2\varepsilon_h}. \quad (2)$$

Rearranging and carrying out some mathematical manipulation, the effective dielectric function ε_{eff} of the system and polarizability are given by

$$\varepsilon_{eff} = \varepsilon_h \left(\frac{1 + 2f\alpha_{eff}}{1 - f\alpha_{eff}} \right), \quad (3)$$

where f is the filling factor of the core-shell NPs defined by

$$f = \frac{4\pi r_s^3}{3} N, \quad (4)$$

and α_{eff} the dimensionless effective electric polarizability of the inclusion given by

$$\alpha_{eff} = \frac{\varepsilon_I - \varepsilon_h}{\varepsilon_I + 2\varepsilon_h}. \quad (5)$$

In the same analogy of effective dielectric function, the effective magnetic permeability of composite material and the dimensionless magnetic polarizability is given by (Kinde, *et al.*, 2021; Liao, 2011):

$$\mu_I = \mu_s \left[\frac{\mu_c \left(\frac{3}{\beta} - 2 \right) + 2\mu_s}{\mu_c + \mu_s \left(\frac{3}{\beta} - 1 \right)} \right]. \quad (6)$$

Using the Clausius-Mossotti relation and the Maxwell-Garnet mixing theory, the magnetic polarizability and permeability are related by (Starodubtcev, *et al.*, 2013; Jackson, 1999; Liao, 2011)

$$\frac{N\kappa_m}{3} = \frac{\mu_{eff} - \mu_h}{\mu_{eff} + 2\mu_h}, \quad (7)$$

where μ_{eff} is the effective magnetic permeability of the ensemble. After some manipulation, we obtained

$$\mu_{eff} = \mu_h \left(\frac{1 + 2f\kappa_{eff}}{1 - f\kappa_{eff}} \right), \quad (8)$$

where $f = 4\pi N a_s^3/3$ is the filling factor of the core-shell NPs and κ_{eff} the dimensionless magnetic polarizability which is given by

$$\kappa_{eff} = \frac{\mu_I - \mu_h}{\mu_I + 2\mu_h}. \quad (9)$$

Optical Responses of Fe_3O_4@Ag Core-Shell Nanocomposites

In this Section, we present the equations for the optical parameters, i.e., the absorption, scattering, and extinction cross-sections with the help of the polarizability equations for a system composed of Fe_3O_4@Ag core-shell NPs embedded in a liquid/water medium. Hence, in order to get an explicit expression for the absorption and scattering cross-sections, we must fix the dielectrics and effective electric and magnetic polarizabilities of the system that consists of the magnetic core, metallic shell, and host matrix.

The response of 'bare' metallic (Ag) shell to incident electromagnetic wave (EMW) is solely described by the dielectric function (permittivity) with the permeability being equal to unity ($\mu_s = 1$). Therefore, we choose the frequency dependent complex dielectric function of the metallic (Ag) shell to have the Drude form given by

$$\varepsilon_s(\omega) = \varepsilon_\infty - \frac{\omega_p^2}{\omega(\omega + i\gamma)}, \quad (10)$$

where the constant ε_∞ is the permittivity at high frequencies, ω_p is the plasma frequency, γ is the damping parameter, and ω is the frequency of the incident radiation. Further, separating the real and imaginary parts of Eq. (10), i.e., $\varepsilon_s = \varepsilon_s' + i\varepsilon_s''$, we obtain the following:

$$\varepsilon_s'(\omega) = \varepsilon_\infty - \frac{\omega_p^2}{\omega^2 + \gamma^2}, \quad (11)$$

and

$$\varepsilon_s''(\omega) = \frac{\gamma\omega_p^2}{\omega(\omega^2 + \gamma^2)}, \quad (12)$$

where $\varepsilon_s'(\omega)$ and $\varepsilon_s''(\omega)$, respectively, are the real and imaginary parts of $\varepsilon_s(\omega)$.

It was well understood that the dielectric function of metals, specifically that of noble and alkali metals, vary significantly as a function of the frequency of the incident light in the visible spectral region, but that of magnetite is constant or vary very little. Hence, we assumed that both the permittivity (ε_c) and permeability (μ_c) of magnetite as well as the permittivity of the host (ε_h) to be real constants independent of frequency.

Effective Electric and Magnetic Polarizabilities

The effective (dimensionless) electric polarizability of the system is given by (Kinde, *et al.*, 2021; Gashaw, *et al.*, 2019; Leta, *et al.*, 2015)

$$\alpha_{eff} = 1 - \frac{3}{2}\vartheta. \quad (13)$$

where,

$$\vartheta = \frac{\varepsilon_c\varepsilon_h + \varepsilon_s\varepsilon_h\left(\frac{3}{\beta}-1\right)}{\varepsilon_c\varepsilon_h + \varepsilon_s\varepsilon_h\left(\frac{3}{\beta}-1\right) + \varepsilon_c\varepsilon_s\left[\frac{3}{2\beta}-1\right] + \varepsilon_s^2},$$

and the corresponding electric polarizability becomes

$$\alpha_e = 4\pi a_s^3 \alpha_{eff}. \quad (14)$$

Because ε_{eff} for the system is complex, the effective electric polarizability α_{eff}, defined by Eq. (13) is also complex, which may be written as

$$\alpha_{eff} = \alpha'_{eff} + i\alpha''_{eff}, \quad (15)$$

where α'_{eff} and α''_{eff} are its real and imaginary parts, respectively. Substituting $\varepsilon_s = \varepsilon'_s + i\varepsilon''_s$ into Eq. (13), we get

$$\alpha'_{eff} = 1 - \frac{3}{2}\xi, \quad (16)$$

and

$$\alpha''_{eff} = \frac{3}{2}\zeta, \quad (17)$$

where

$$\xi = \frac{(\varepsilon'_s\phi' + \varepsilon_c\varepsilon_h)\varphi' + (\varepsilon''_s\phi')\psi}{\varphi^2 + \psi^2},$$

$$\zeta = \frac{(\varepsilon'_s\phi' + \varepsilon_c\varepsilon_h)\psi - (\varepsilon''_s\phi')\varphi'}{(\varphi)^2 + \psi^2},$$

$$\phi' = \varepsilon_h\left(\frac{3}{\beta} - 1\right),$$

$$\eta = \phi' + \varepsilon_c\left(\frac{3}{2\beta} - 1\right),$$

$$\varphi' = (\varepsilon_s)^2 - (\varepsilon''_s)^2 + \varepsilon_s\eta + \varepsilon_c\varepsilon_h,$$

$$\psi = 2\varepsilon_s\varepsilon''_s + \varepsilon''_s.$$

Similarly, substituting Eq. (6) into (9), we find the effective magnetic polarizability to be

$$\kappa_{eff} = 1 - \frac{3}{2}\left[\frac{\mu_c\mu_h + \mu_s\Delta}{\mu_c\mu_h + \mu_s\Delta + \mu_c\phi + \mu_s^2}\right], \quad (18)$$

where

$$\Delta = \mu_h\left(\frac{3}{\beta} - 1\right),$$

and

$$\phi = \mu_s\left(\frac{3}{2\beta} - 1\right).$$

In particular, for the case where μ_c is a real constant and $\mu_s = \mu_h = 1.0$ (nonmagnetic), we find that Eq. (18) for the dimensionless polarizability reduces to

$$\kappa_{eff} = 1 - \left[\frac{3+\beta(\mu_c-1)}{\mu_c+2}\right], \quad (19)$$

and the corresponding magnetic polarizability becomes

$$\alpha_m = 4\pi a_s^3 \kappa_{eff}. \quad (20)$$

Note that both κ_{eff} and α_m of Eqs. (19) and (20) are real constants.

Absorption, Scattering, and Extinction Cross-Sections

The absorption cross-section, σ_{abs}, of the system consisting of spherical core-shell composite NPs embedded in a host matrix is given by (Leta, *et al.*, 2015):

$$\sigma_{abs} = k\,\mathrm{Im}[\alpha_e + \alpha_m], \quad (21)$$

where $k = 2\pi\sqrt{\varepsilon_h}/\lambda$. Note that α_m is a real constant.

In addition, we consider that the loss of electromagnetic wave upon propagation through the spherical nano-inclusions results by means of the generation of heat and scattering. The scattering cross-section, σ_{sc}, of the system can be shown to have the following form:

$$\sigma_{sc} = \frac{k^4}{6\pi}|\alpha_e + \alpha_m|^2. \quad (22)$$

Furthermore, the extinction cross-section, σ_{ext}, of the system is given by

$$\sigma_{ext} = \sigma_{sc} + \sigma_{abs}, \quad (23)$$

where σ_{sc} and σ_{abs} are given by Eqs. (21) and (22), respectively.

RESULTS AND DISCUSSION

Next, we numerically analyzed the polarizability as well as the absorption, scattering, and extinction cross-sections of the theoretically modelled spherical Fe_3O_4@Ag core-shell NPs embedded in a dielectric host matrix. These optical parameters are analyzed by varying the material parameters β and ε_h). For the numerical evaluations, we used Mathematica version 10 software. The following parameter values are used in the simulation: $\varepsilon_\infty = 4.5$, $\omega_p = 1.46 \times 10^{16}\, rad/s$ and

$\gamma = 1.67 \times 10^{13}\ rad/s$ for the silver shell; and $\varepsilon_c = 5.85$ and $\mu_c = 9.0$ for magnetite.

Absorption Cross-Section

The absorption cross-section of Fe_3O_4@Ag core-shell spherical nanoinclusions are numerically analyzed using Eq. (21) together with the corresponding expressions for α_e and α_m, i.e., Eqs. (14) and (20). The absorption cross-section (σ_{abs}) of the spherical nano-inclusions as a function of the wavelength of the incident EMW for different values of β and ε_h at a fixed value of NPs size $a_s = 10\ nm$ as shown in the Figs. 2a) and 2b). The graphs possess two sets of resonance peaks – the first set of peaks in both cases are located in the vicinity of $\lambda = 300$ nm in the UV region which are attributed to the interaction at the inner (Fe_3O_4/Ag) interface. The second set of peaks are found above the wavelength of $\lambda = 450$ nm all in the visible spectral region, which corresponds to the resonances at the outer (Ag/host) interface. As β increases (or equivalently as core radius a_c decreases), the two sets of peaks gets far apart from each other accompanied with a spectral shift towards lower wavelengths in the first set of peaks and shifted to the higher wavelengths in the second set of peaks (see Fig. 2a)). The peak values of σ_{abs} are found to be more pronounced in the second set of peaks than the first set of peaks.

As it seen from the graphs, the effect of a rapid onset of strong absorption, occurring in the UV regions for all dielectric medium/host ε_h, is dependent on the particles size. That is, when the value of β is increased, the absorption peaks sharply drops (less intense) for both the first and second peaks (see Fig. 2a) for a constant $\varepsilon_h = 1.77$. On the other hand, for a particular value of $\beta = 0.725$, the absorption cross-section for both the first and second sets of peaks sharply increases as ε_h increases and red-shifted as shown in Fig. 2b.

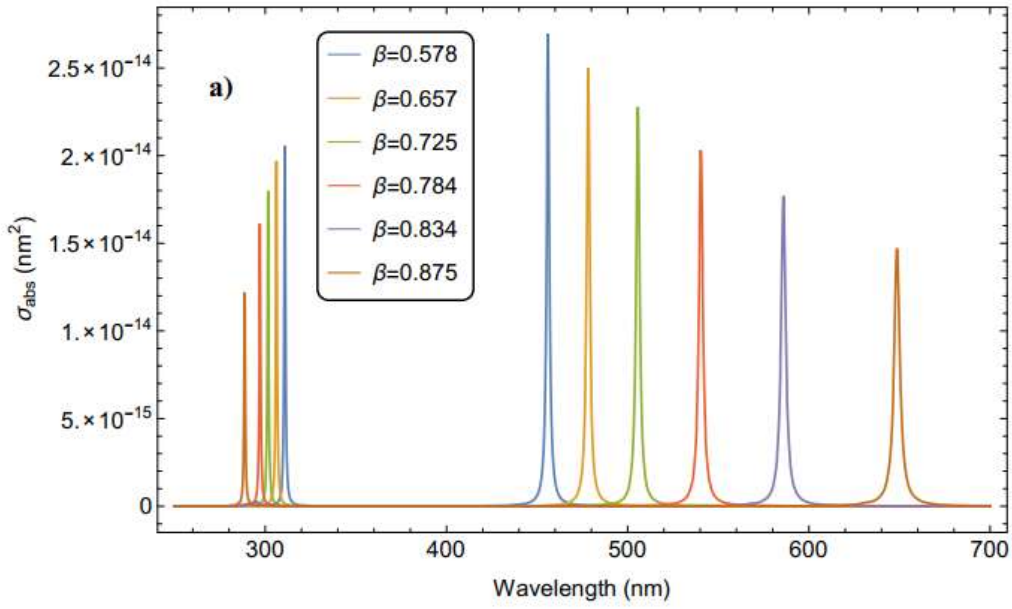

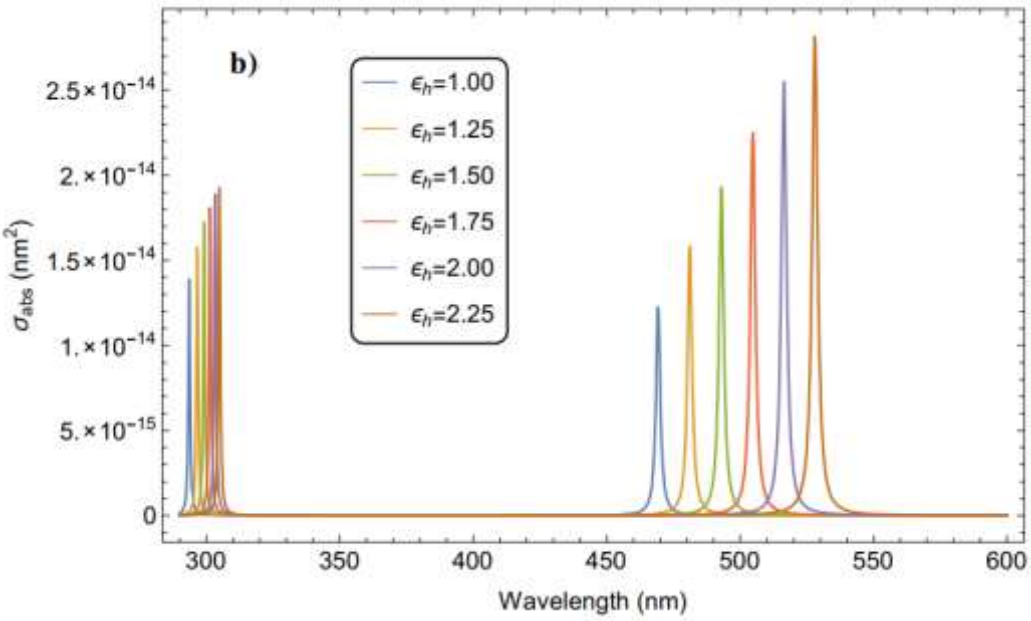

Figure 1. The absorption cross-section versus wavelength a) for different values of β and b) for different values of ε_h; with $f = 0.003$ and $a_s = 10$ nm.

Scattering Cross-Section

Figures 3a and 3b depicts the size dependent scattering cross-section (σ_{sca}) of the spherical $Fe_3O_4@Ag$ nano inclusions as a function of the wavelength of the incident electromagnetic waves (EMWs) for different values of β and ε_h and a fixed value of QD size a_s = *10 nm*. In each figures there are two sets of resonance peaks. The first set of resonance peaks positioned near to $\lambda = 300$ nm in the UV region and is associated with the inner (magnetite/Ag) interface. The second set of peaks which are connected to Ag/host interface are located above the wavelength of $\lambda = 450$ nm all in the visible spectral region. Figure (3a) illustrate that, scattering of light is sharply increased (more scattering takes place) in the first set of peaks than the second set of peaks and gets sharply decreased as β increases. Furthermore, the two sets of peaks increases as ε_h increases as shown in the Fig. 3b. From both Figs. 3a and 3b, it is observed that the first resonance peaks are more pronounced than the second set of peaks. As the size of the system of core-shell nanoparticles gets smaller and smaller, the metal fraction, β, is also decreased. This leads to the decrease in the scattering cross-sections.

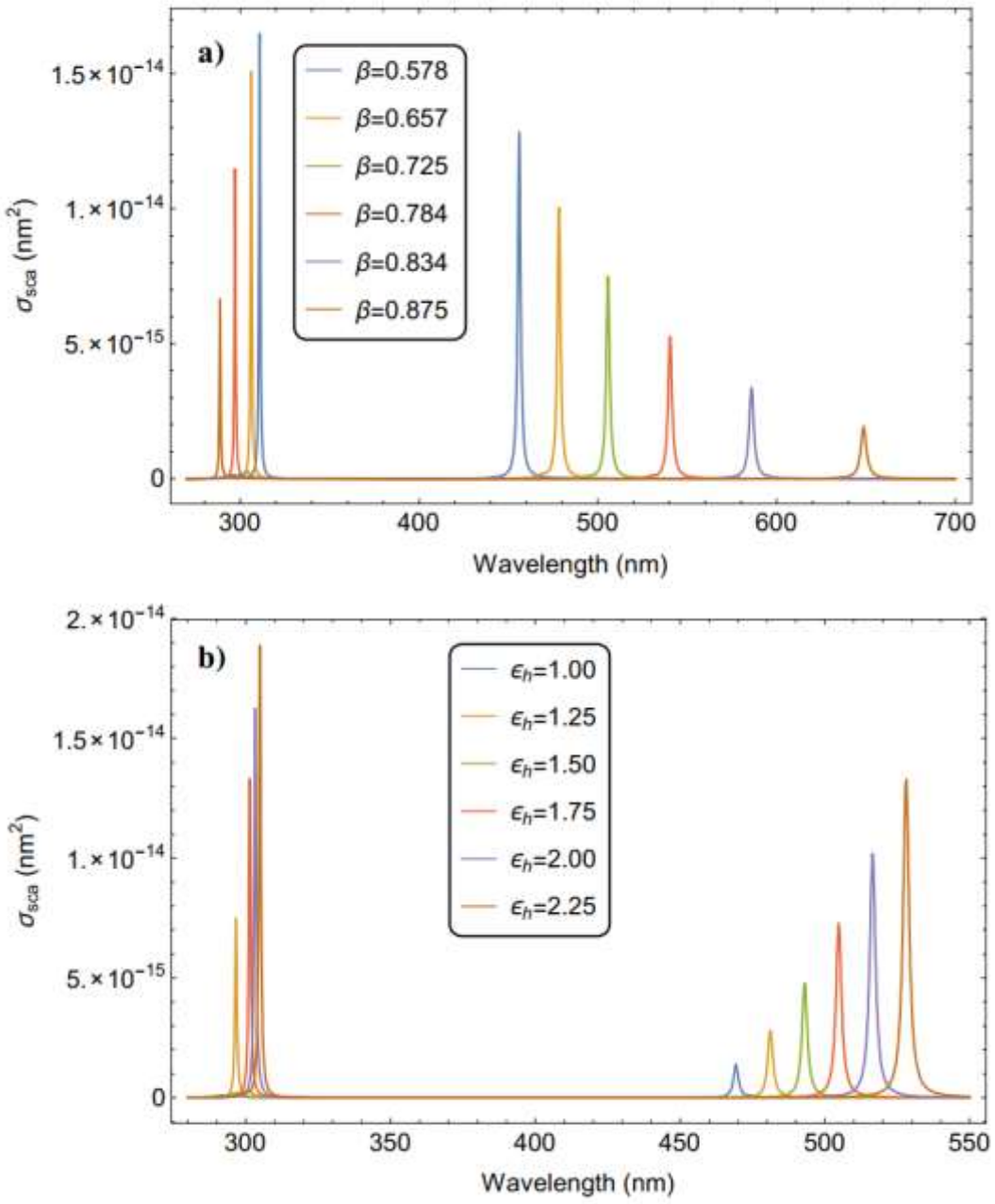

Figure 2. The scattering cross-section as a function of wavelength a) for different values of β and b) for different values of ε_h; with fixed values of $f = 0.003$ and $a_s = 10$ nm.

In Fig. 3a, the two sets of resonances gets closer each other as β decreases accompanied by the shift towards the higher energy in the second peaks and emission spectral shift to lower energy in the first peaks. Both sets of resonance peaks are red-shifted (see Figs. 3) as ε_h increased. For both figures 3a and 3b there are no noticeable peaks found in the first sets of peaks at particular values $\beta = 0.725$ and at $\varepsilon_h = 1.50$. This may be due to the fact that, the absorption is more likely to dominate over scattering processes at the particular values of $\beta = 0.725$ and at $\varepsilon_h = 1.50$. On the other hand, the dielectric medium at the value of $\varepsilon_h = 1.50$ in the host matrix may affect the propagation of the incident electromagnetic wave.

Extinction Cross-Section

Figures 4 depict the graphs of extinction cross-section, σ_{ext} as a function of wavelength for different values of β and ε_h for the spherical

nanoinclusions. As it is seen from the graphs, the extinction cross-section possess two sets of resonance peaks. The first set of peaks for Figs. 4a and 4b, the resonance peaks are located close to $\lambda = 300$ nm in the UV region and the first set of peaks are due to resonances at the inner (magnetite/Ag) interface. The second set of peaks are those found above the wave length of about $\lambda = 450$ nm all in the visible spectral region.

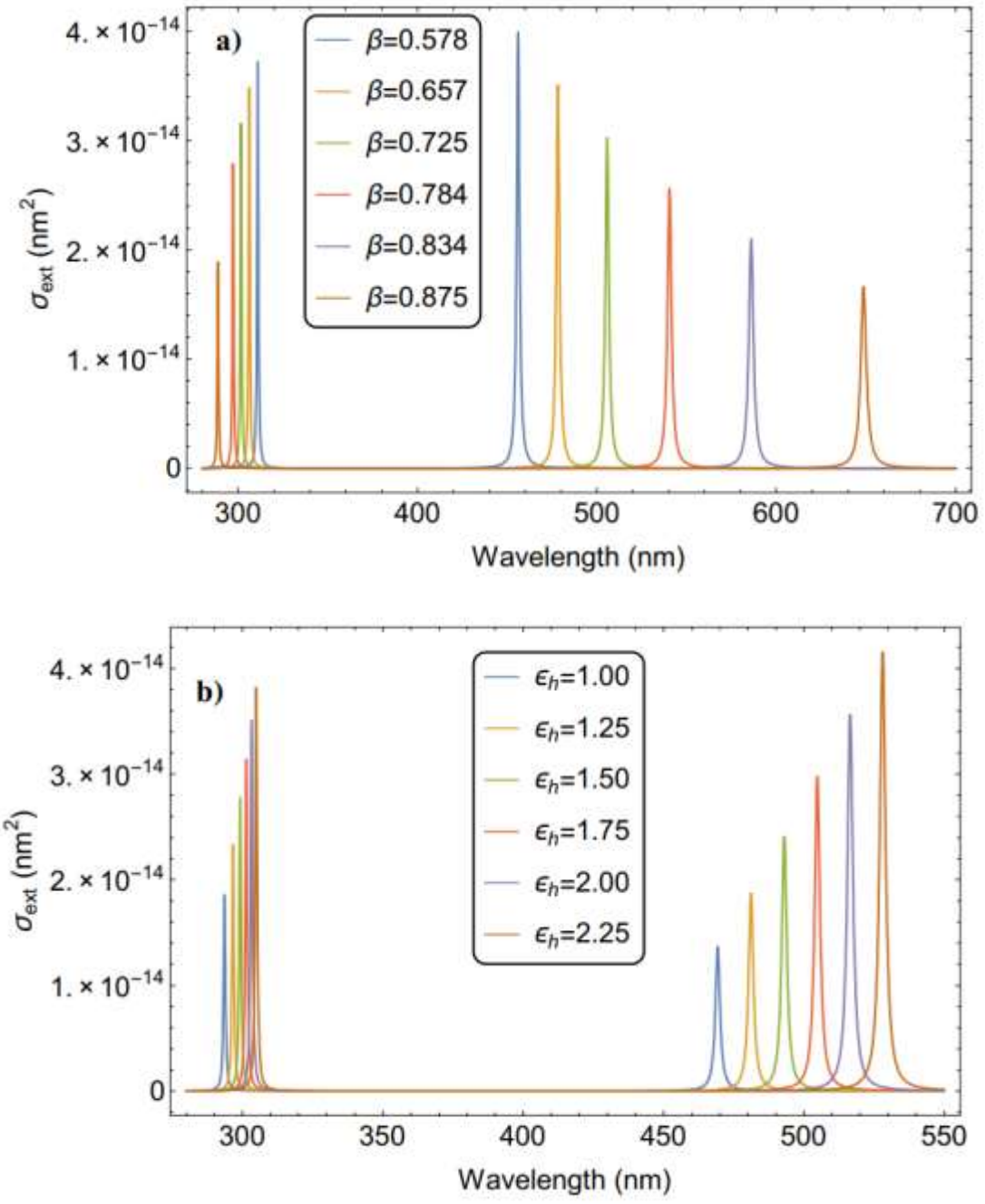

Figure 3. The extinction cross-section versus wavelength for different values of a) β and b) ε_h; with fixed values of $f = 0.003$ and $a_s = 10$ nm.

As Fig. 4a) depicts, the two sets of resonances gets closer to each other as β is decreased and the spectra shift towards lower frequencies in the first set of peaks, and shift toward higher frequencies for the second set of peaks. Both sets of resonance peaks are red-shifted (see Fig. 4b) as ε_h is increased.

The extinction cross-section depends on the chemical composition of the particles, their size, shape, orientation, the surrounding medium, the number of particles, and the polarization state and frequency of the incident EMWs (Bohren, 1998). The system of spherical core-shell nanoparticles that is considered in this study is composed of two chemically dissimilar nanoparticles - one as the semiconducting core and the other as a plasmonic shell. We found that the extinction cross-section is dependent on the size and chemical composition of the semiconducting core or the metallic shell.

As the results depict in Fig. 2 and Fig. 3, the absorption cross–section dominates over the scattering cross–section. Since the extinction cross–section is the combined effect of both absorption and scattering cross–sections, the two sets of resonance peaks gets more pronounced (see Fig. 4.).

CONCLUSIONS

In this study, we investigated the effects of varying parameters like the metal fraction and host matrix on the systems of spherical core-shell Fe_3O_4@Ag nanoparticles embedded in a dielectric host matrix. It is found that the absorption cross-section, scattering cross-section as well as the extinction cross-section of the system plotted for different values of β and ε_h as a function of wavelength possess two sets of resonance peaks in the UV (in the vicinity of $\lambda \sim 300$ nm) and visible (above $\lambda \sim 450$ nm) spectral regions. These sets of peaks arise due to the coupling of the surface plasmon oscillations of silver with the energy gap of the semiconducting core at the inner (Fe_3O_4/Ag) interface and at the outer metal/dielectric (Ag/host matrix) interface. Moreover, when β is increased, the first set of peaks in the UV region are which is mainly attributed the decrease of the size of the semiconducting Fe_3O_4 core, while the second set of peaks are in the visible regions with an increase of β, due to an increase in the thickness of the metallic Ag shell. For the graphs of absorption and scattering cross-sections the first set of resonance peaks are shifted towards higher frequencies as β increases.

Furthermore, the graphs of the absorption and scattering cross-sections for different values of the metal fraction β and at a constant dielectric function of the host matrix (for fixed $\varepsilon_h = 1.77$) possess two set of peaks - the first in the UV (around $\lambda \sim 300$ nm) and the second in the visible (above $\lambda \sim 420$ nm) spectral regions. Both sets of resonance peaks are enhanced accompanied with a red and blue shift. In the same manner, it is found that with an increase in the permittivity ε_h of the host, the resonance peaks are enhanced accompanied with a red shift. In this case, both sets of peaks are shifted to higher wavelength with an increase in ε_h.

Finally, the enhancement of the optical properties of the system (spherical core-shell Fe_3O_4@Ag nanoparticles embedded in a dielectric host matrix) is because of the strong coupling of the surface plasma oscillations of the silver shell with the energy gap of the magnetic semiconducting (Fe_3O_4@Ag) nano-core. It means that the silver nanoshell strongly modifies the optical properties of Fe_3O_4 nanoparticles which correspondingly modify its potential applications. The results obtained may be utilized in device fabrication and applications that integrates the plasmonic effects of noble metals with magnetic semiconductors such as Fe_3O_4 in core-shell nanostructures.

REFERENCES

1. Ahmad, Y. M. (2015). Light trapping effect in plasmonic blockade at the interface of *Fe_3O_4@Ag* core-shell. *RSC Adv, 5*, 40989.
2. Ana, O. R.-J. (2019). Development of Multifunctional Liposomes Containing Magnetic/Plasmonic *$MnFe_2O_4$/Au* Core-Shell Nanoparticles. *Pharmaceutics, 11*(10).
3. Bohren, C. F. (1998). *Absorption and Scattering of Light by Small Particles* (1st ed. ed.). Weinheim: Wiley-VCH. doi:ISBN 978-0-47-129340-8.
4. Challa, S. (2013). *UV-Vis and PL Spectroscopy for Nanomaterials Characterizations.* Berlin Heidelberg: Springer-Verlag.
5. Chang, H.-M. a. (2011). A Parallel Derivation to the Maxwell-Garnett Formula for the Magnetic Permeability of Mixed Materials. *World Journal of Condensed Matter Physics, 1*, 55-58.
6. Chingsungnoen, P. C. (2017). Composite *Fe_3O_4@Au* Core-Shell Nanoparticle: Tunable and Enhancement of Optical Absorption Property. *Oriental Journal of Chemistry, 33*(4), 1642-1647.
7. Ezequiel, R. E. (2013). Synthesis of Ag@ZnO core-shell hybrid nanostructures: an optical approach to reveal the growth mechanism. *Journal of Nanoparticle Research, 15*, 1688.

8. Fan, W. Z. (2019). Effect of component volume ratio on the absorption spectra of $Ag@Fe_3O_4$ core-shell nanoparticles. *Modern Physics Letters B, 33*(7), 1950071.

9. Gashaw Beyene, T. S. (2019). Size dependent optical properties of ZnO@Ag core-shell nanostructures. *Chinese Journal of Physics, 58*, 235-243.

10. Jackson, J. (1999). *Classical Electrodynamics* (3^{rd}. Ed. ed.). J. Wiley and Sons Inc.

11. Kerker, M. (1969). *The Scattering of Light and Other Electromagnetic Radiation* (1^{st} ed. ed.). New York, New York, USA: Academic Press.

12. Kheradmand, E. P. (2020). Optical and magnetic properties of iron-enriched $Fe/Fe_xO_y@Au$ magnetoplasmonic nanostructures. *Applied Nanoscience*.

13. Kinde yeneayehu, T. S. (2021). Enhancement of the optical response of $Fe_3O_4@Ag$ core-shell nanoparticles. *Physica E: Low Dimensional Systems and nanostructures, 134*, 114822.

14. Leta Jule, V. M. (2015). Fano-like resonance and scattering in dielectric(core)/metal(shell) composites embedded in active host matrices. *Phys. Status Solidi B, 252* (12), 2707 - 2713.

15. Luciano, C. F. (2013). Waste Water – Treatment Technologies and Recent Analytical Developments: Applications of Magnetite Nanoparticles for Heavy Metal Removal from Wastewater.

16. Maria, E. F. (2014). Compact $Ag@Fe_3O_4$ Core-shell Nanoparticles by Means of Single-step Thermal Decomposition Reaction. *Scientific Reports* (4), 683.

17. Morones, J. R. (2005). The bactericidal effect of silver nanoparticles. *The bactericidal effect of silver nanoparticles. Nanotechnology, 16*(10), 2346-2353.

18. Papavassiliou, C. (1979). Optical properties of small inorganic and organic metal particles. *Prog. Solid State Chem, 12*, 185271.

19. Poedji L. H., M. F. (2013). Synthesis and Properties of Fe_3O_4 Nanoparticles by Co-precipitation Method to Removal Procion Dye. *International Journal of Environmental Science and Development, 4*(3).

20. Shweta, B. J. (2019). Near-field and far-field optical properties of magnetic plasmonic core-shell nanoparticles with non-spherical shapes: Adiscrete dipole approximation study. *AIP Advances*.

21. Starodubtcev, S. E. (2013). Reduced polarizability and local-field effect in self assembled ensemble of nanoparticles. *J. Nano-Electron. Phys., 5* (1), 1 - 5.

22. Vladimir, V. A. (2013). Unusual application of common digital devices: Potentialities of Eye-One Pro mini-spectrophotometer A monitor calibrator for registration of surface plasmon resonance bands of silver and gold nanoparticles in solid matrices. *Sensors and Actuators B, 188*, 1109-1115.

23. Vollmer, U. A. (1995). *Optical Properties of Metal Clusters* (1st ed. ed.). Heidelberg: Springer. doi:ISBN 978-3-642-08191-0

24. Xu, R. M. (2009). Ag nanoparticles sensitize IR-induced killing of cancer cells. *Cell Research, 19*(8), 1031-1034.